

## EMIR performances after detector upgrade

**Garzón, F.<sup>1,2</sup>, Fernández–Acosta, S.<sup>3</sup>, Hammersley, P.<sup>4</sup>, Joven, E.<sup>1,2</sup>, Rodríguez, H.<sup>1,2</sup> Russo, A.<sup>3</sup> and Rosich, J.<sup>1,2</sup>**

<sup>1</sup> Instituto de Astrofísica de Canarias, La Laguna, Spain

<sup>2</sup> Departamento de Astrofísica, Universidad de La Laguna, Spain

<sup>3</sup> European Southern Observatory, Garching bei München, Germany

<sup>4</sup> GRANTECAN S.A., La Palma, Spain

### Abstract

EMIR was shipped to the GTC on May 2016 and had its first light on June 2016. After a short and intense commissioning period, a Scientific Verification phase took place in the first half of 2017 and the instrument began its routinely operation at the GTC by the end of that year. Since the beginning, the EMIR performances have been severely hampered by the many instabilities in the infrared detector, a  $2048 \times 2048$  Hawaii2, built with the old original technology of the Teledyne Hawaii series. Despite of this, the instrument has proven to be powerful enough so as to produce a significant number of important scientific contributions. Starting in 2020, we initiated a new project aimed at equip EMIR with a most modern detector array, free from the artefacts that contaminated the observations with the old one. As a results, and after almost 6 years of routine operations at the GTC, EMIR has recently been upgraded with a new Hawaii2RG infrared detector which has replaced the old Hawaii2 that equipped the instrument in origin. The new detector is not only more sensitive in virtually every aspect compared to the old one, but it also eliminates many of the instabilities of the original detector that severely hindered EMIR's performance., while it is not free from artefacts that affect the noise in the measurements. This is particularly noticeable under high illumination conditions, i.e. broad band imaging, as it will be shown below. In addition, the new detector sits on a remotely operated gimbal mount that permits an exquisite alignment in the field of view. In this contribution, we will describe the capabilities of the new EMIR and will show some fresh scientific results, and will also flag some features that users should be aware of.

## 1 Introduction

EMIR [2] [3] is a near-infrared multi-object spectrograph operating in the range of 1 to 2.5  $\mu\text{m}$ , which form part of the suite of common user instruments in the GTC. EMIR (Espectrógrafo Multiobjeto InfraRojo, Multi-object Infrared Spectrograph) has been developed mainly at the IAC, with the participation of the UCM (Madrid) and the French institutes Observatoire de Toulouse and Observatoire de Marseille. Wide-field image and multi-object and long-slit spectroscopy observation modes are available, with spectral resolutions between 1000 and 5000. For more details, refer to the instrument web sites at the IAC and GRANTECAN. Its first light took place in mid-2016, although the commissioning of the different observation modes lasted until well into 2018, given the high complexity of the systems that equip the instrument. As of that date, we began an intense scientific verification campaign that revealed, in addition to the capabilities of the instrument, the need to replace the detector, which is too noisy and unstable, with another of the latest generation. To this end, we started in 2021, right after the pandemic, the tasks aimed at equipping the instrument with a most modern detector array, a Hawaii2RG. Together with the replacement of the detector itself, we also added the substitution of the Gimbal mount’s angle adjustment micrometer screws with new piezoelectric actuators that can be remotely operated once the system had been cooled down. This last task resulted in the complete redesign and building of a new detector mount on which the actuators can be integrated. The new detector was received by the end of 2022 and accepted at the IAC after a test campaign on which the top-level requirements were verified.

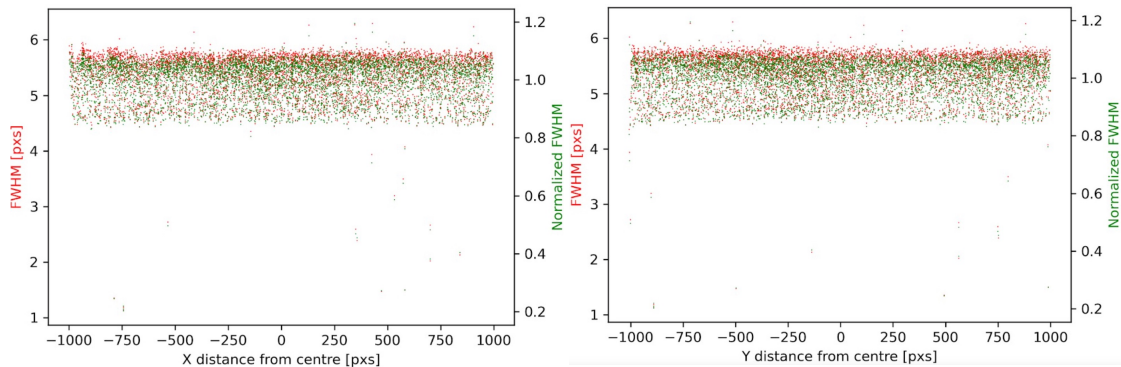


Figure 1: FWHM of point-like sources in several open clusters taken with EMIR in the J band. In red, absolute FWHM figures vs X, left panel, and Y, right panel, distances from the detector centre. In green, FWHM values are normalised to the mean of the full set.

To this end, we started in 2021, right after the pandemic, the tasks aimed at equipping the instrument with a most modern detector array, a Hawaii2RG. Together with the replacement of the detector itself, we also added the substitution of the Gimbal mount’s angle adjustment micrometer screws with new piezoelectric actuators that can be remotely operated once the system had been cooled down. This last task resulted in the complete redesign and building of a new detector mount on which the actuators can be integrated. The new detector was

received by the end of 2022 and accepted at the IAC after a test campaign on which the top-level requirements were verified.

By May 2023, EMIR was sent off its location at the Nasmyth platform of the GTC to the clean room within the premises of the telescope at the summit. Then, the instrument was disassembly to a level on which the Detector Translation Unit (DTU) housing the detector mounting could be dismantled. The new detector unit, sited in the motorized Gimbal mount, was then attached to the DTU, aligned and integrated back into its position at the instrument optical bench. Several quick functional tests were run before cooling down and also after cooling, at cryogenic temperatures, to ensure the correct working of the detector and mount before warming up the instrument to proceed to install it back at the Nasmyth rotator.

## 2 First on sky results

In August 2023, we started observing in a series of technical nights dedicated to asses and measure the real performance of the new detector and of the instrument in general. At first, we proceeded aligning the tilt angles of the mount with respect to the instrument focal surface. In Figure 1 we show the how, after the alignment process, the detector surface alignment is extremely parallel to the instrument focal surface, as the image size shows a high uniformity across the full field of view.

Together with an excellent alignment, the detector also shows a remarkable good photometric uniformity and sensitivity. Figure 2 depicts a deep image taken with EMIR in the J band of Abell 370, with very little data treatment, that can be compared with the same field in a multicolour image from the HST. The initial measurement of the photometric zero point was performed by taking images of several open clusters with seven dither point pattern. Part of the image series are displayed in Figure 3, where several flaws in the image frames can be seen. In particular, vertical stripes with different background levels due to the detector readout structure are not properly treated. Also, black areas surrounding some target objects are clearly visible. These are due to imperfections in the image reconstruction from the dither pattern. At the time of this writing, part of these flaws are fixed in the new versions of the reduction pipeline (PyEmir). Only the targets squared in green in Figure 3 are used to maintain uniformity, as the external parts are not in common to all the seven dither pointings. The sources are distributed all over the frame and it is of note the high concentration of values around the mean. Table 1 shows the measured ZP in the JHKs bands compared with the same figures with the old detector. To transform from counts to electrons, we have used the gain measured in laboratory test of 3.3 e-/adu, while this value is yet a bit uncertain as we have obtained slightly different ones in different measurements, using several data treatment schemes. It has to be mentioned that there still artefacts in the detector readout scheme, that will be referred to in the next section, that have some influence in the photometry. We are currently working on eliminating these effects that would result in even better improvement of the sensitivity. For the time being, and as it will be shown below, the way we are alleviating these instabilities consists mainly in reducing the detector duty cycle. We have not yet repeated these photometric observations with this method implemented. Summing up all the improvements from the time of the original observations and

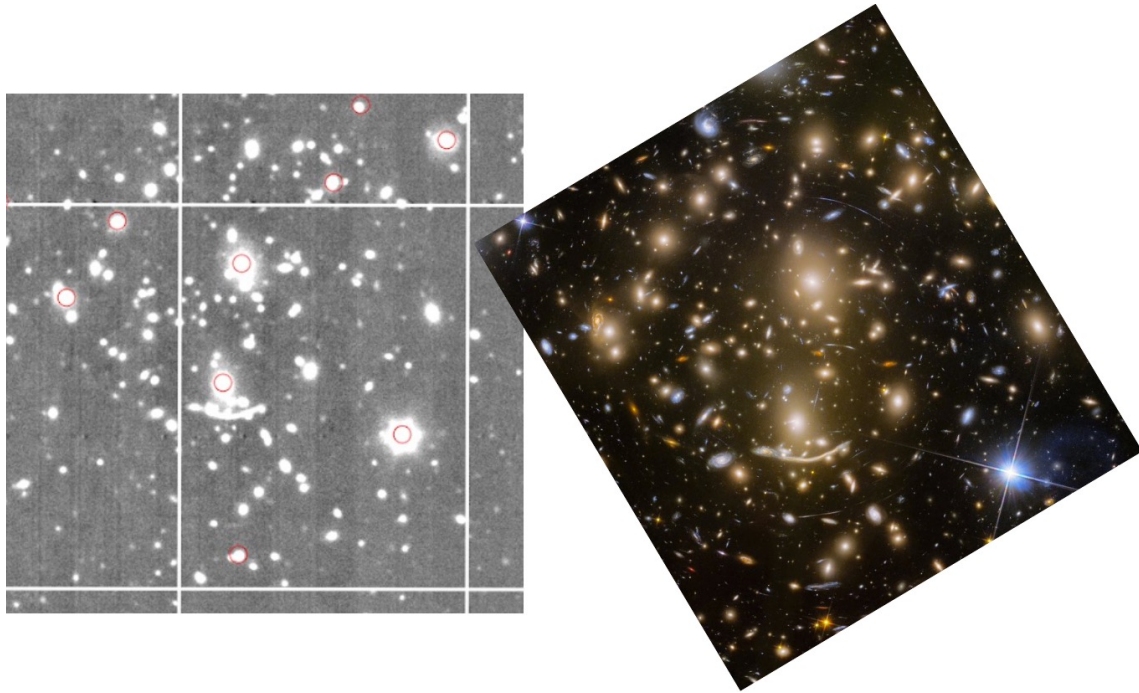


Figure 2: Central region of the cluster of galaxies Abell 370. The EMIR J image, on the left, has been produced combining 400 CDS images, 10s each; on the right, a HST Frontier Field multicolour image of the same cluster, for comparison purposes. Red circles on the EMIR image are the positions of the GAIA DR3 sources found on the field.

data reduction, it is expected that the final ZPs will beat the values in Table 1.

We have also taken a series of measurements of dark current at the detector, consisting in long integration times with the instrument fully closed (entrance window, Cold Slit Unit, grism wheel, filter wheel). Results are given in Figure 4 , that shows that there is no real impact of the working temperature of the detector in this range between 40K and 60K. Due to better behaviour with respect to persistence, we are operating the detector at 40K. In the same set of measurements, we have obtained a figure for a readout noise in single read of  $20.12e^-$  as a mean value over the 32 outputs of the array.

### 3 Non linear effects in detector

Non-linear effects in the conversion from charge to voltage, and then to counts, in the near infrared detectors are well known since long ago (see for example [4] and [5] ), and several methods to correct them can be found in the literature. In Figure 5, we show how this effect is present in the EMIR H2RG and one potential method to account for it. In Figure 5, blue diamonds represent the raw data, red squares are the fit to the ramp following the prescription in [5] and the green symbols depict the linear part of the previous fits. As can be seen, non-linear effects are only important with high signal levels, and standard correction

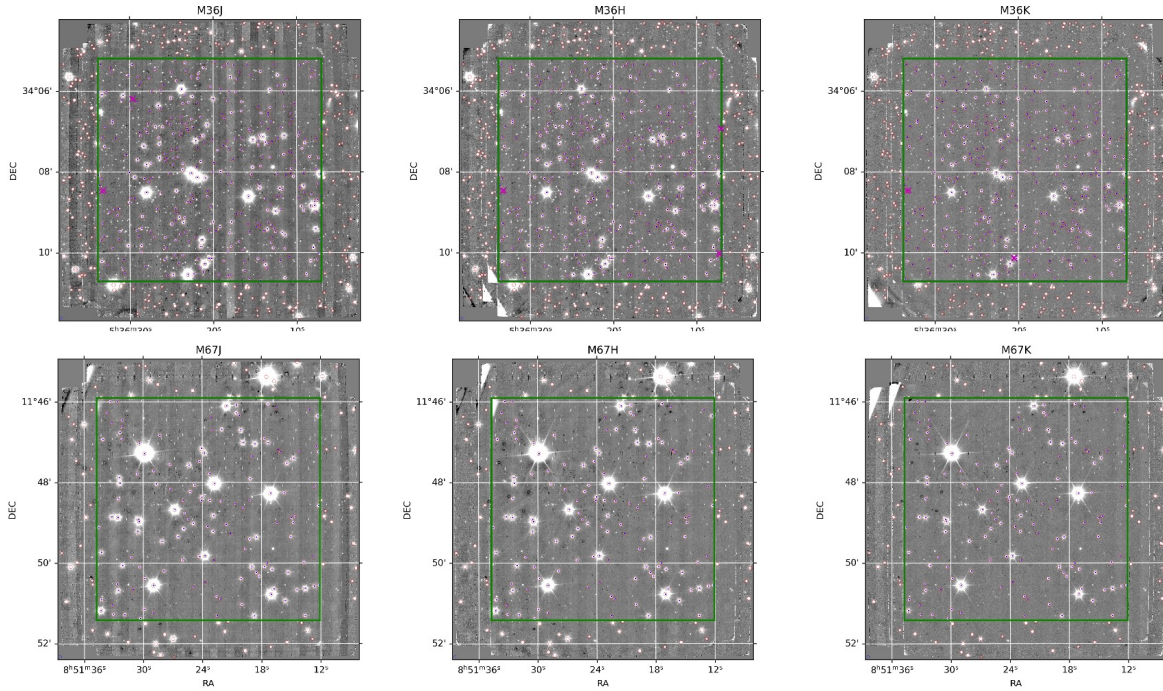


Figure 3: JHKs images of two open clusters used to derive the sensitivity of the instrument. See text for details. Red circles on the EMIR image are the positions of the GAIA DR3 sources found on the field.

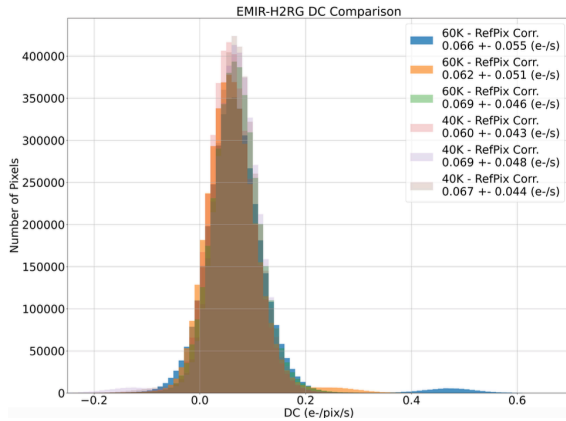


Figure 4: Several histograms of Dark Current at two detector temperatures, 40K and 60K. No significant differences are observed. Current operational temperature of the EMIR H2RG is 40K.

Table 1: Zero points measured in telescope using open clusters M36 & M67 photometry. In parentheses, the magnitudes with the old detector.

Band	mag@1adu/s	mag @1e <sup>-</sup> /s
<i>J</i>	25.570 ± 0.179 (25.14)	26.848
<i>H</i>	25.746 ± 0.101 (25.26)	26.942
<i>K<sub>s</sub></i>	25.203 ± 0.176 (24.81)	26.476

can produce non desirable results in low flux cases. That shows that, as expected, non linear effects are more acute under high illumination.

It is important for a multipurpose instrument like EMIR to correct this effect, as the broad band image mode can collect several thousand counts per second just from the thermal emission of the atmosphere, the redder the band the higher the counts. So, in CDS readout mode (*Correlated Double Sampling*, a variation of *Fowler* sampling with one read per group), which is the EMIR standard for image mode, the cost of non correcting the lack of linearity in the measurement will result in a loss of signal. The plan to deal with this effect, following [5], is to derive a non-linearity correction using well defined ramps, in URG read mode, that can be applied when only two read frames are available, as the in the CDS read mode. We are working with several schemes to apply this correction. At this time, the best results are obtained deriving a ratio of non linearity (RNL) on each pixel, grouping different measurements with similar illumination levels, and obtain RNL polynomial fit per pixel and flux range that can be later be applied to the raw measurements. This procedure is extremely costly in terms of computational resources and we are working along different lines that would permit to alleviate this burden. Averaging pixels per readout channel is one of the most promising areas of development. There are also useful hints in [https://nexsci.caltech.edu/committees/JWST/smith\\_bright\\_objects.pdf](https://nexsci.caltech.edu/committees/JWST/smith_bright_objects.pdf).

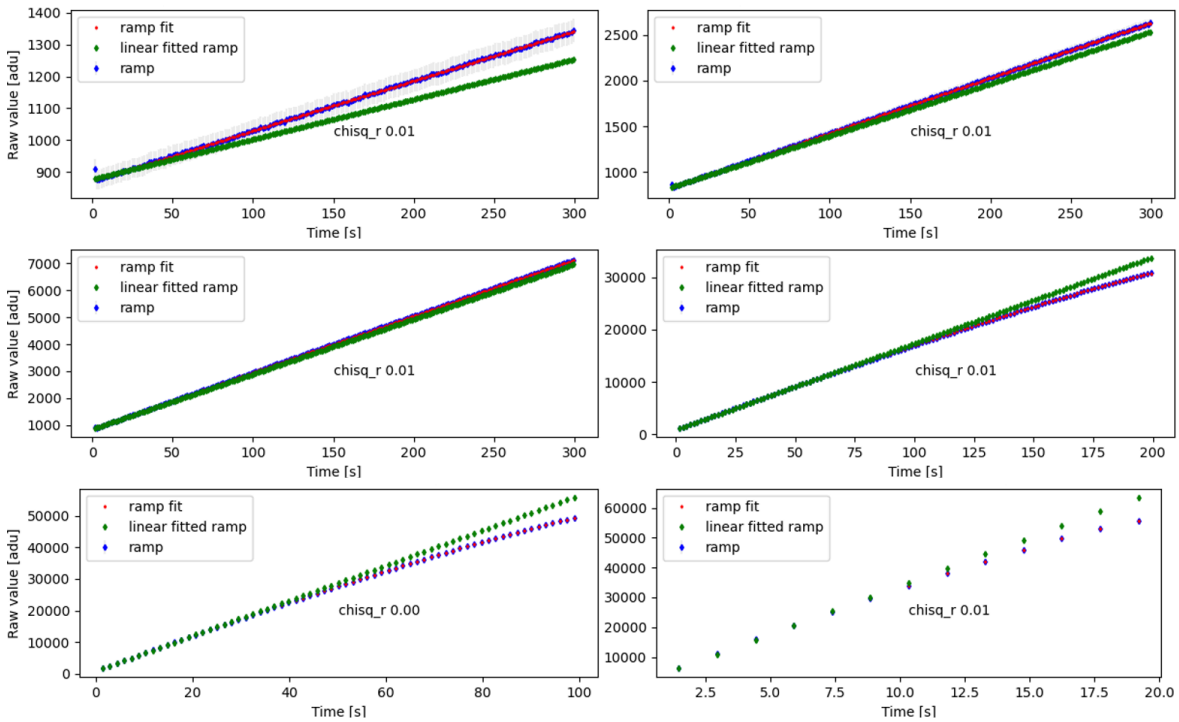


Figure 5: Ramps taken at different illuminations, with increasing incoming flux left to right, top to bottom.

## 4 Drift in signal after reset

The most harmful effect in the detector signal that we have observed so far is an offset seen in the raw counts in both read modes, URG (*Up the Ramp*) & CDS, when taking a series of ramps in a sequence. The offset in slope can be as high as few kadu/s, depending on incoming flux, between the first ramp and the rest of the sequence. The offset is more noticeable in the raw counts of the frame taken immediately after the last reset, but translate also to the final slope, while at smaller level. We have performed many tests, that are still ongoing, that demonstrate that the offset has more to do with the illuminating flux and less with the time from the last reset. In fact, using the smallest portion of the detector frame that permits the current detector controller, so as the readout time is very short compared with the full detector frame time, we have verified that this effect is still present. So, it seems not to depend on the time between last reset and first read, which is rather short in this case.

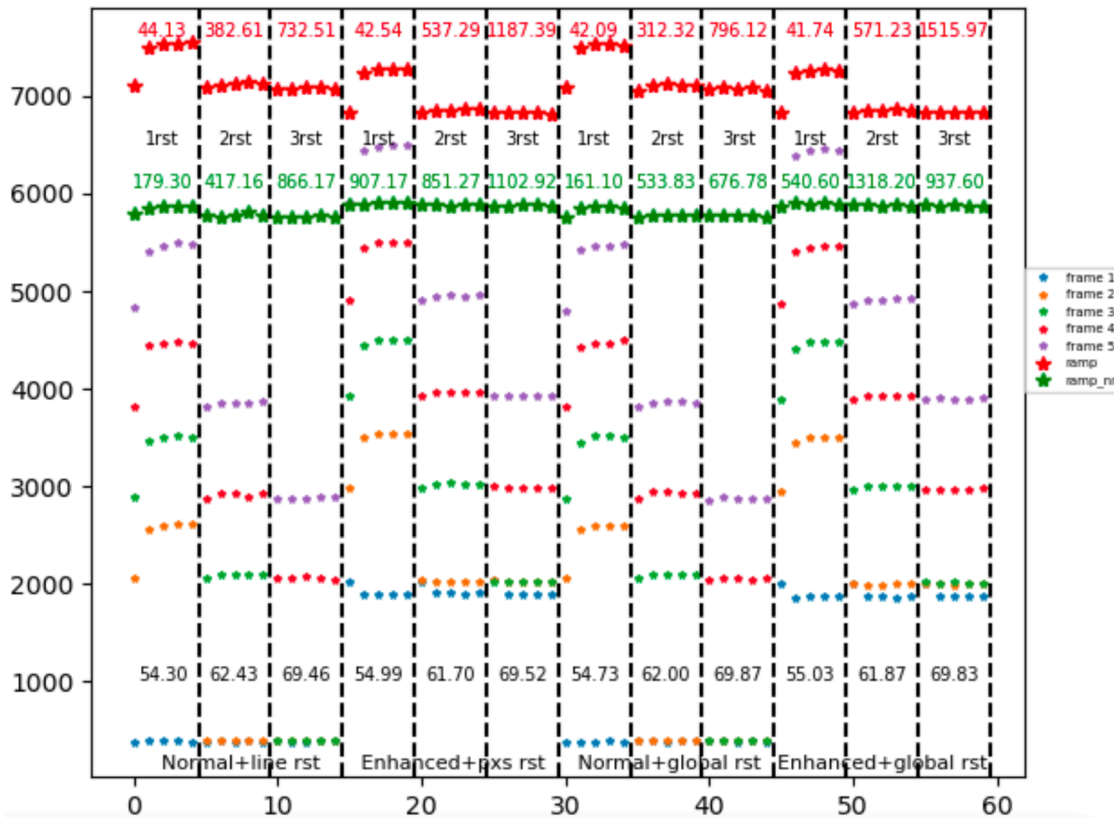


Figure 6: Sequences of 5 ramps, 5 reads each, covering all the reset types and with 1 to 3 resets before reading

In Figure 6 we show this effect in a series of measurements. We cover the complete set of reset types available in the existing *firmware* of the detector controller, that are given in the text at the bottom. Per reset type, we take 3 sequences of 5 ramps each, separated 3 minutes in time, and with a number of resets after each ramp on the sequence varying from

1 to 3. Each point in Figure 6 is derived by averaging a central section of 200x2040 pxs on each frame. Big red asterisks in Figure 6 show the initial signal of each ramp obtained by a linear fit on the full frame sequence. It is remarkable the difference between the first ramp and the rest of the sequence in the 1 reset series. This difference becomes smaller as the number of resets increases and virtually disappear with 3 resets per ramp. The red number on top of each sequence represents a sort of signal to noise ratio, as it is the mean value divided by the standard deviation of the signals. Big green asterisks in Figure 6 show the same magnitudes previously described, but after removing the initial jump on each ramp. In this case, the drift effect decreases but are still present. Moreover, the signal fluctuates heavily depending on the input flux, effect that cannot be seen in Figure 6, and the results are not reliable. As it is clear that several resets are needed to stabilise the signal, we are currently evaluating ways of implementing fast reset in the existing control infrastructure. With the current detector driver, the reset time equals the frame readout time, significantly impacting duty cycle efficiency when multiple resets are performed before each integration sequence. Currently, the default reset sequence includes two resets in CDS and three resets in URG readout modes.

## 5 Conclusions

In summary, EMIR is now in a significantly more capable state compared to before the commencement of operations to replace the detector, install the DA remote control, and perform maintenance on the CSU. However, some actions remain pending, notably the fine calibration of the CSU, which has not yet been completed due to technical issues, and improvements to the detector's readout procedure. Having a high-speed reset procedure is a priority in this regard. These fast resets can be implemented in the H2RG (see for example [6]) but would surely require different *firmware* to be installed in the detector controller.

Finally, we are also working on refining the image reduction methods to adapt them to the new characteristics, as well as addressing some minor unwanted effects, such as non-linearity under high-signal regimes.

## Acknowledgments

EMIR has been funded by GRANTECAN S.L. via a procurement contract; by the Spanish funding agency grants AYA2001-1656, AYA2002-10256-E, FIT-020100-2003-587, AYA2003-01186, AYA2006-15698-C02-01, AYA2009-06972, AYA2012-33211, AYA2015-63650-P and AYA2015-70498-C2-1-R; and by the Canarian funding agency grant ACIISI-PI 2008/226. This work has been partly supported by project AYA2018-RTI-096188-B-I00.

## References

- [1] Canipe, A., Robberto, M. and Hilbert, B. 2017 Technical Report JWST-STScI-005167, SM-12.

- [2] Garzón, F. & EMIR Team 2016, Multi-Object Spectroscopy in the Next Decade: Big Questions, Large Surveys, and Wide Fields, 507, 297.
- [3] Garzón, F., Balcells, M., Gallego, J., et al. 2022, *A&A*, 667, A107.
- [4] Plazas, A. A., Shapiro, C., Smith, R., et al. 2017, *Journal of Instrumentation*, 12, C04009.
- [5] Robberto, M. 2011 Technical Report JWST-STScI-002344.
- [6] Storz, C., Naranjo, V., Mall, U., et al. 2012, *Proceedings of the SPIE*, 8453, 84532E.